University of Bath

Alternative formats

If you require this document in an alternative format, please contact:
openaccess@bath.ac.uk

DATA INFORMED MODEL TEST DESIGN WITH MACHINE LEARNING – AN EXAMPLE IN NONLINEAR WAVE LOAD ON A VERTICAL CYLINDER

A PREPRINT

Tianning Tang
Department of Engineering Science,
University of Oxford,
Oxford, OX1 3PJ, UK
email: tianning.tang@eng.ox.ac.uk

Haoyu Ding
Department of Architecture and Civil Engineering,
University of Bath,
Bath, BA2 7AY, UK
email: hd484@bath.ac.uk

Saishuai Dai
Naval Architecture, Ocean and Marine Engineering Department,
University of Strathclyde,
Glasgow, G1 1XQ, UK
email: saishuai.dai@strath.ac.uk

Xi Chen
Department of Computer Science,
University of Bath,
Bath, BA2 7AY, UK
email: xc841@bath.ac.uk

Paul H. Taylor
Oceans Graduate School,
The University of Western Australia,
35 Stirling Highway,
Crawley, WA 6009, Australia
email: paul.taylor@uwa.edu.au

Jun Zang
Department of Architecture and Civil Engineering,
University of Bath,
Bath, BA2 7AY, UK
email: jz235@bath.ac.uk

Thomas A. A. Adcock
Department of Engineering Science,
University of Oxford,
Oxford, OX1 3PJ, UK
email: thomas.adcock@eng.ox.ac.uk

September 23, 2023

ABSTRACT

Model testing is common in coastal and offshore engineering. The design of such model tests is important such that the maximal information of the underlying physics can be extrapolated with a limited amount of test cases. The design of experiments also requires considering the previous similar experimental results and the typical sea-states of the ocean environments. In this study, we develop a model test design strategy based on Bayesian sampling for a classic problem in ocean engineering – nonlinear wave loading on a vertical cylinder. The new experimental design strategy is achieved through a GP-based surrogate model, which considers the previous experimental data as the prior information. The metocean data are further incorporated into the experimental design through a modified acquisition function. We perform a new experiment, which is mainly designed by data-driven methods including several critical parameters such as the size of the cylinder and all the wave conditions. We examine the performance of such a method when compared to traditional experimental design based on manual decisions. This method is a step forward to a more systematic way of approaching test designs with marginally better performance in capturing the higher-order

force coefficients. The current surrogate model also made several 'interpretable' decisions which can be explained with physical insights.

Keywords Fluid-Structure Interaction, Machine learning, Hydrodynamics

1 Introduction

Offshore wind turbine foundations are exposed to the hazardous ocean environment and must be designed to survive the ultimate loads. For the wave loading on the monopile foundations, the relatively small Keulegan-Carpenter (KC) number indicates that for non-breaking waves, inertial loading tends to dominate the total inline forcing and it is common to neglect the drag force effect. Nonlinear physics further introduces higher-frequency components, which could contribute significantly to the total inline force for very steep and nonlinear waves. The linear part of the inertial loading has the same frequency as the incoming wave field, which by design is away from the typical structural natural frequency of monopile foundations (around two or three times the frequency of severe storm waves (1)). These higher-frequency harmonics, however, can be much closer or even overlap with the structural natural frequency. This overlap is of concern to the structural and geotechnical design of the monopile foundations and can potentially lead to the excitation of a structure resonance, which is usually referred to as 'ringing effect' (2; 3; 4).

Various theoretical works have looked at these higher order harmonics (5; 6; 7; 8). Experiments and numerical simulations (9; 10) are also used to further explore the underlying physics of these higher-order harmonics, including our recent work, where a phase decomposition method is applied to further separate the higher frequency components from the linear loading and Stokes type force expansion is used to predict the higher frequency forces as a nonlinear function of the linear loading in time (11; 12; 13).

In addition to the theoretical derivations, various numerical and experimental works have also investigated wave interaction with a vertical cylinder (14; 15; 2; 9; 3; 16). Marino et. al. investigated the nonlinear wave loads for irregular waves (17), and Schløer et. al. further considers the aero-hydro-elastic calculations (18). Ghadirian and Bredmose (18) investigated the 'strong' nonlinear physics beyond higher order harmonics.

With the increasing number of experiments and numerical datasets produced at various laboratories and research groups, the new experiential design should be based on various pieces of information together to further explore the underlying nonlinear physics. This includes a consistency check against previous experimental data and suggestions for new experimental cases to explore the parameter combinations that are not covered by previous experimental cases, aiming at improving the overall model accuracy over a wide range of sea states. Additionally, new cases should be representative of real sea-state conditions in the operational wind farm.

Rather than relying on physical intuition or past experience, a systematic experimental design strategy is preferred to address these challenges. In this study, we take a data science approach to design our new experiment and use Bayesian interference as a small step forward. The Bayesian interference is a widely used optimisation tool in computer science and machine learning (19). Recent studies in ocean engineering (20; 21; 22) also further utilised this technique to design numerical simulations based on previous results, which can lead to a significant saving of computational resources with a properly designed sequential sampling strategy.

In this study, we performed an experiment that is primarily designed by machine learning at the University of Strathclyde. A surrogate model based on Gaussian Process is used to interpolate previous experimental results and a new acquisition function is proposed to integrate metocean data from the ECWMF dataset. The proposed design strategy allows the integration of different types of information: experiments, and metocean data to assist the decision-making process in the design of new experiments. This model provides information to assist the choice of several critical experimental parameters including the size of the cylinder and all the wave conditions. We compare the performance of the proposed model against the traditional experimental design strategy and observed some improvement in the final predictions of nonlinear loading on a vertical cylinder.

We structure this paper as follows. We first introduce the experimental setup in section 2 and provide a brief introduction of the metocean and experimental data used in this study in sections 3 and 4. We then provide details of the machine learning models in sections 5 and 6 and present results in section 7.

2 Experimental setup

In this paper, we aim at designing a new set of experiments in the large flume (76 m long, 4.6 m wide with a constant water depth of 1.8 m) at the Kelvin Hydrodynamics Laboratory, the University of Strathclyde. We are primarily interested in the nonlinear wave loads on a single bottom-mounted surface-piercing vertical cylinder placed 35.3 m

away from the wavemaker. There is a parabolic beach at the far end of the flume away from the wavemakers for wave absorption. Reflections from the beach are expected, however, the reflected wave packets reach the cylinder at a later time and are excluded from the analysis. Hinged-flap type wavemakers are installed at the other end of the flume. Linear wave generation theory was applied, and the impact of second-order error waves on the overall wave loading was analysed carefully. We can also confirm that the second-order error wave packet is separated from the main group at the time of interaction with the cylinder.

In this study, we are primarily interested in focused wave groups, which are also interconnected with the averaged shape of the largest events in the random time series (according to NewWave theory (23; 24)). The focus point of these wave groups is at the centre of the cylinder. In the experiments, the waves are generated based on the JONSWAP spectrum (25) with peak enhancement factor, $\gamma = 3.3$. As the wave group propagates along the wave tank, significant nonlinear evolution is expected for steep wave groups (26; 27; 28). Local properties of wave group profiles at focus are measured without the presence of the cylinder and are used for further analysis. Wave breaking occasionally occurs before the wave group arrives at the position of the cylinder and these cases are excluded from our analysis. The Keulegan-Carpenter number for most of the experimental cases for the current study is less than 5, which means the load is inertial load dominated. The KC number is computed by $KC = \pi A/R$, where A to be the linear focused wave amplitude, R is the cylinder radius.

3   Previous experiments

Datasets obtained from the previous three experiments are used as the prior information for guiding the design of this new experimental campaign (details are given in (12; 13; 11)). Similar focused wave group profiles were generated during these experiments with the same JONSWAP spectrum ($\gamma = 3.3$) but with different peak periods and amplitudes. The relative water depths and the cylinder sizes also vary due to the physical constraints in the experimental facilities. The detailed design of these experiments in terms of three non-dimensional parameters (k_A, $k_p d$ and $k_p R$) is given in Figure 7, where k is the peak wavenumber, A is the wave group amplitude at the focus point if the wave evolves linearly, d is the water depth of the flume and R is the radius of the cylinder. The similar experimental setup and wide range coverage of these previous experimental data provide the basic information to start the design of our new experimental campaign.

All the experiments including the previous and current cases are primarily focused on the unidirectional wave conditions (except for (11) where spreading sea states are also considered), which is different for the directionally spread waves in the open ocean (29).

4   Metocean data

Realistic environmental data is critical to the design of new experiments as these data provide information on the typical sea-states which are representative of ocean environments where offshore wind turbines are and will be constructed in the near future. The design of new experiments should be tailored to metocean data to avoid any cases that are unlikely to occur in realistic sea states.

In this study, we obtain the metocean data from the ERA5 dataset from ECWMF (30). We have downloaded the sea-states parameters at 36 current and potential locations of offshore wind farms around UK, as shown in Figure 1. The use of all past locations of offshore wind farms may introduce a bias towards smaller monopile sizes and shallower water depths compared to the next phase of installations, which can be further mitigated when more information about the next generation of offshore wind turbine installation information is available. The resolution of ocean wave data is $0.5°$ x $0.5°$ and the nearest node to the location of the wind farm is used for the analysis herein. Rigorous data quality control and validation of this dataset has been done previously in (30) and missing entries are carefully checked throughout. In this study, we are primarily interested in three metocean parameters: significant wave height (H_s), hourly maximum wave height (H_{max}) and peak period (T_p). We have collected the hourly variation of these three data at all 36 wind farm locations between the period of 2004 and 2024, which contains a total of 87600 hourly sea-states. We have also collected the monopile size information and the averaged water depth of the wind farm from the company official or project website for these 36 UK based wind farms.

We also performed a data pre-filtering to these collected sea-states, where only 50% of sea-states with large (based on H_{max}) and 50% sea-states with long waves (based on T_p) are considered (see Figure 2 for details). The threshold for this pre-filtering is arbitrary and we do not account explicitly for the correlation between H_{max} and T_p but is a compromise based on the limited availability of experimental facilities. More sophisticated pre-filtering can be easily adapted into the framework depending on the source of the field data. We focus on long waves due to their importance in ultimate loading calculations on monopile design (31), and among these long waves, sea-states with higher amplitude

waves are considered as the nonlinear wave-wave interactions are more pronounced for steeper wave groups (12). These cases are favoured given limited tank time in terms of both scientific interests and the importance of extreme loading conditions during severe winter storms. Additionally, the wavemaker also struggles for high frequency wave groups, where the accuracy of the wave generation is more of a concern. We also note that such pre-filtering is not critical for the current proposed experimental design method and potential improvements will be further discussed in section 7.3.
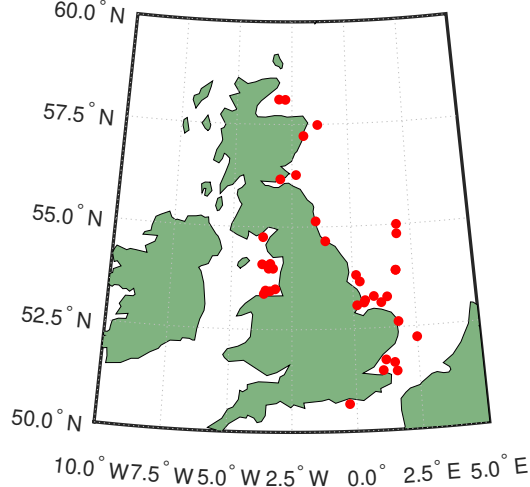

Figure 1: Site map for 36 locations of UK-based wind farms.

5 Gaussian Process as a surrogate model

To separate the nonlinear loading on a vertical cylinder from the linear components, we use a four-phase harmonic extraction method (32). This method is also used in previous studies (12; 13), which decomposes nonlinear forces into different harmonics in frequency by repeating the experiments with four different phases (see Eqn 2 in (13) for details). These decomposed higher-order frequency components can be further fitted based on the linear force envelope raised to the appropriate power. The fitted amplitude and phase coefficients can be used to predict the nonlinear force inertial loading on a vertical cylinder based on linear wave force only.

Further to the four-phase decomposition method, we use the Stokes-type force model to predict these higher-order forces following (12). Under the narrow-banded spectrum assumption, the waves can be assumed to be associated with a slowly varying wave envelope $\hat{\mathcal{F}}_1$, and the total wave force up to the 4th harmonic can be expressed as:

$$F = \hat{\mathcal{F}}_1 \cos(\varphi) + \hat{\mathcal{F}}_1^2 F_2 \cos(2\varphi + \Phi_2) + \hat{\mathcal{F}}_1^3 F_3 \cos(3\varphi + \Phi_3) +$$

$$\hat{\mathcal{F}}_1^4 F_4 \cos(4\varphi + \Phi_4) + O\left(\hat{\mathcal{F}}_1^5\right) \quad (1)$$

where $\mathcal{F}_1$ is the envelope, φ is the phase of the higher order forces, and F_n is the amplitude coefficients for the nth order of force harmonics and Φ_n is the corresponding phase coefficients.

The force amplitude coefficients $F(x)$ depend on three non-dimentionalised parameters k_A, $k_p d$ and $k_p R$. Previous experiments only cover part of the parameter space, leaving some of the area uncovered. As such, new experiments are required to further explore the force amplitude coefficients variation in the parameter space to improve the nonlinear inline forces prediction accuracy.

We model the variation of these coefficients with a Gaussian Process (GP) using a mean function $m(x)$ and a covariance function $k(x, x^*)$:

$$\begin{aligned} F(x) &\sim \mathcal{GP}\left(m(x), k\left(x, x^*\right)\right) \\ m(x) &= \mathbb{E}[F(x)] \\ k\left(x, x^*\right) &= \mathrm{cov}\left(F(x), F\left(x^*\right)\right) \end{aligned} \quad (2)$$
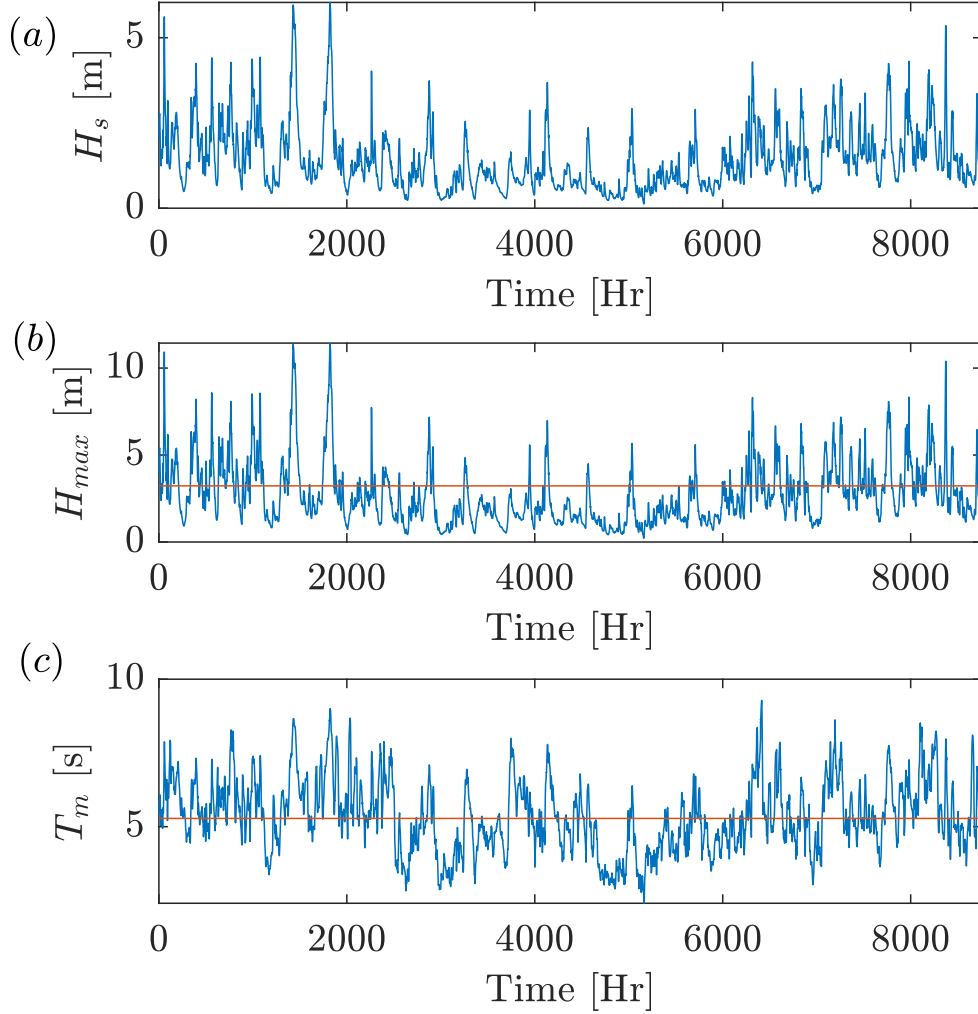
Figure 2: An example of sea-state metocean data obtained from EAR5 dataset from ECWMF for (a): significant wave height, (b): hourly most probable maximum wave height, and (c): peak period. The two red lines indicate the threshold for data pre-filtering, where only 50% of sea-states with large (based on H_{max}) and 50% sea-states with long waves (based on T_p) are considered.

where $x \in (k_p A, k_p d, k_p R) \equiv \mathbf{R}$ is a parameters space input vector with three dimensions, $F(x)$ and $F(x^*)$ are force amplitude coefficients response indexed by x and x^*. Generally, $k(x, x^*)$ is also referred to as a kernel function, which is further parameterised by a hyperparameter θ.

GP is a common Bayesian non-parametric model used for both regressions and parameterisation purposes. This method is particularly suitable in our prediction model because of its strong resistance to under-fitting the problems. In this study, one of the key challenges for the accurate prediction of force coefficients is the limited data available from previous experiments. A GP's expressiveness in proportion to the size and complexity of the growing dataset avoids the under-fitting problem (33) for small datasets. Additionally, the ability to provide uncertainty quantification also favours the wide application of the GP model in many engineering problems, such as system identification (34), control (35) and forecasting (36).

In this study, the variation function of force amplitude coefficients $F(x)$ in parameters space $x \in (k_p A, k_p d, k_p R)$ is assumed to be a complex system without existing expert domain knowledge. For systems without any accurate description of the dynamics model, a GP model is commonly initialised with a zero mean function, which leads to the prior in GP is solely dependent on the choice of the covariance function $k(x, x^*)$. Although the covariance functions

$k(x, x^*)$ are fully customisable for any function, which can provide a positive definite covariance matrix, the selection of this function determines the periodicity and smoothness of the trained GP model. Hence, a suitable covariance function type and hyperparameter θ initial values are required during the initialisation of a GP.

In this study, we follow the most common covariance function: squared exponential, which is also noted as Radial Basis Function:

$$k(x_i, x_j) = h_1^2 \exp\left[-\left(\frac{x_i - x_j}{\lambda}\right)^2\right],$$ (3)

which can be further optimised by using a loss function based on the log marginal likelihood function following (37).

Now we consider the training dataset $S = \left\{\left(x_{(i)}, F_{(i)}\right)\right\}_{i=1}^m$, where m is the number of observations and the testing dataset $T = \left\{\left(x_{(i)}^*, F_{(i)}^*\right)\right\}_{i=1}^{m_*}$, where m_* is the number of prediction points, for notational convenience, we define

$$X = \begin{bmatrix} -(x_1)^T - \\ -(x_2)^T - \\ \vdots \\ -(x_m)^T - \end{bmatrix} \in \mathbf{R}^{m \times n} \quad \vec{F} = \begin{bmatrix} F_1 \\ F_2 \\ \vdots \\ F_m \end{bmatrix} \in \mathbf{R}^m,$$

$$X_* = \begin{bmatrix} -(x_1^*)^T - \\ -(x_2^*)^T - \\ \vdots \\ -(x_m^*)^T \end{bmatrix} \in \mathbf{R}^{m_* \times n} \quad \vec{F}_* = \begin{bmatrix} F_1^* \\ F_2^* \\ \vdots \\ F_{m*}^* \end{bmatrix} \in \mathbf{R}^{m*}.$$ (4)

where $n = 3$ is the number of features. The trained GP model can make the prediction F^* for a new given input X^* based on the extended joint distribution as:

$$\begin{bmatrix} \vec{F*} \\ \vec{F} \end{bmatrix} \sim \left(\begin{bmatrix} m(X^*) \\ m(X) \end{bmatrix}, \begin{bmatrix} K(X^*, X^*) & K(X^*, X) \\ K(X, X^*) & K(X, X) + \sigma^2 I, \end{bmatrix}\right)$$ (5)

where $K(X^*, X) = K(X, X^*)^T = [k(X_1, X^*), \cdots, k(X_m, X^*)]$, σ^2 is the noise variance, and I is the identity matrix, and $K(X, X)$ is expressed

$$K(X, X) = \begin{bmatrix} k(x_1, x_1) & \cdots & k(x_1, x_m) \\ \vdots & \ddots & \vdots \\ k(x_m, x_1) & \cdots & k(x_m, x_m) \end{bmatrix},$$ (6)

where m is the size of the training dataset (i.e. observations), and the rest co-variance matrix can be expressed in a similar manner as:

$$K(X, X_*) \in \mathbf{R}^{m \times m_*} \text{ such that } (K(X, X_*))_{ij} = k\left(x_{(i)}, x_{(j)}^*\right)$$

$$K(X_*, X) \in \mathbf{R}^{m_* \times m} \text{ such that } (K(X_*, X))_{ij} = k\left(x_{(i)}^*, x^{(j)}\right)$$

$$K(X_*, X_*) \in \mathbf{R}^{m^* \times m^*} \text{ such that } (K(X^*, X^*))^{ij} = k\left(x_{(i)}^*, x_{(j)}^*\right).$$ (7)

According to the properties of joint Gaussian distributions, the prediction results for the outputs can be obtained as:

$$\mu\left(\vec{F*}\right) = m(X^*) + K(X^*, X)\left[K + \sigma^2 I\right]^{-1}(Y - m(X))$$

$$\text{var}\left(\vec{F*}\right) = K(X^*, X^*) - K(X^*, X)\left[K + \sigma^2 I\right]^{-1}K(X, X^*),$$ (8)

where $\mu(F^*)$ is the predicted force amplitude coefficients and $\text{var}(F^*)$ is the variance of the predicted force amplitude coefficients (see an example of GP prediction in Figure 3).
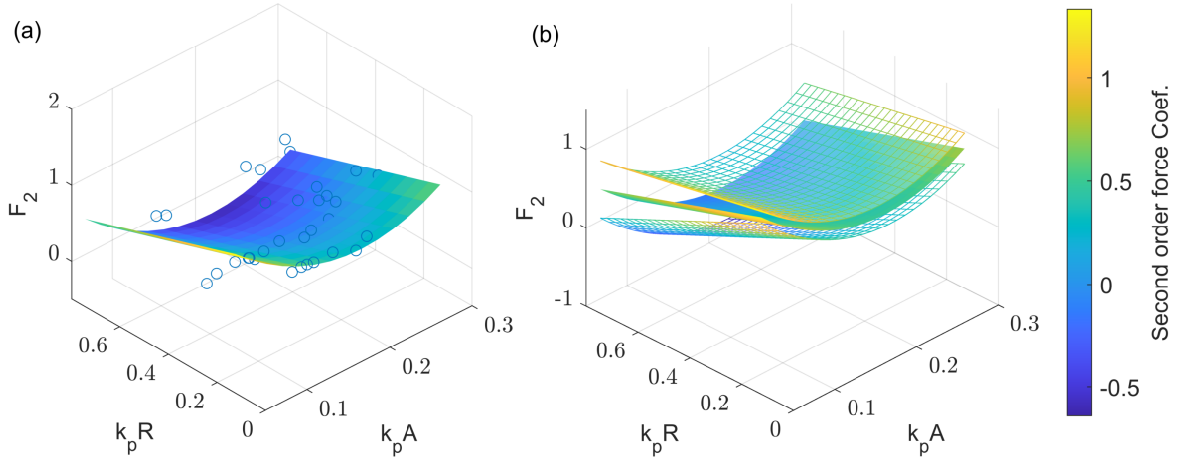
Figure 3: An illustration of prediction from GP as a surrogate model for second order force coefficients for (a) prediction residual and (b) confidence interval. Blue circles represent the previously acquired sampling points via experiments.

For a limited size of dataset, the random split of the training and validation data may also introduce bias in the prediction results. To minimise the impact of this split, a bootstrapped k-fold cross-validation process (38) is applied to further examine the accuracy of our GP model. In this study, the dataset is uniformly divided into n subsets and $n-1$ uniform-sized subsets are used for GP model training. The performance of the currently trained GP model can be evaluated by validating against the out-of-bag sample. After repeating the training and validation process covering all the data points as the out-of-bag sample, the overall performance measurements can be calculated as the average of across the k-folds. The k-folds validation is a common cross-validation method that repeats model training with different parts of data, which can maximize both training and testing data and also give a better idea of how well the model will perform on unseen data (38).

6   Acquisition function

Uncertainty sampling is a common active sampling method, which locates the next best sampling point ($\hat{x}$) to be the position where the predictive variance achieves a maximum value:

$$\hat{x} = \text{argmax}_{x \in (k_p A, k_p d, k_p R)} \text{var}[(F^*)]. \tag{9}$$

This acquisition function is easy to use and particularly useful when limited data are available (20). However, for this particular engineering problem, the acquisition function requires further modification as the largest uncertainly will inevitably occur at the parameter space $x \in (k_p A, k_p d, k_p R)$ where the test case can not be physically achieved (i.e. too steep waves locally exceeded the breaking limits), as shown in Figure 3 (b) as an example.

Hence, we further modify the likelihood-weighted acquisition functions proposed in (39) to incorporate the conditional statistics calculated from Section 4 as:

$$\hat{x} = \text{argmax}_{x \in (k_p A, k_p d, k_p R)} \text{var}[(F^*) \, w(x)], \tag{10}$$

where the $w(x)$ is the conditional statistics estimated from the probability of such a combination of parameters occurring at the location of UK-based wind farms, which can be visualised in the bin scatter plot in Figure 4. This acquisition function allows direct assimilation and integration of the field data into the experimental design, which provides realistic oceanographic conditions.

We note that the current experimental campaign also benefits from batch sampling as the automated wave generation system allows performing experiments overnight. The data analysis and surrogate model training, however, still require manual supervision. Batching the experimental design for running overnight provides more observations over a limited tank time slot. As such, we follow the batching procedure suggested in (40) in searching for sub-optimal sampling points at multiple local minima of the acquisition function.

To find multiple regions with local optima from the acquisition function, a condition that no Bayesian sample may occur closer than a specified distance is introduced (40) as:

$$r_{\min} = r_l \left(\sum_{d=1}^{N_D} (x_{d,+} - x_{d,-})^2 \right)^2, \tag{11}$$

where $x_{d,+}$ and $x_{d,-}$ are the maximal and minimal domain bounds (i.e. the maximum and minimum value of $k_p A, k_p d, k_p R$ that is achievable with the current experimental setup), and r_l is a user-defined percentage, where we choose a static value of $r_l = 0.05$ and N_D is the batch size which is 45 due to the physical constraints of the current experimental setup. Trading marginally reduced performance with more completed experiments is beneficial to the experimental campaign overall.

7 Results

In this section, we will first summarise the typical sea-states at 36 locations of UK-based offshore wind farms. We will then reveal the ML interpretation of the best design of the current experimental campaign and compare the performance against the traditional grid search method.

7.1 Metocean data

We present the distribution of hourly sea-states parameters (i.e. H_s, H_{max} and T_p) for all 36 locations of UK offshore wind farms in Figure 4. We have also calculated the peak wavenumber k_p based on the finite depth dispersion relationship with the averaged water depth information of the local wind farm. We also approximate the amplitude (A) of the hourly maximum wave as the half of the maximum wave height (H_{max}), as the wave height distributions are less affected by the second order bound waves (41).

From Figure 4, we found that the majority of sea-states for UK-based wind farms are in finite water depth with the relative water depths $k_p d < 3$. This is expected as other configurations of wind turbines such as the floating turbines would be preferred for deeper water locations. The striped pattern is also clear from the $k_p d$ vs. $k_p R$ plot, which is primarily due to the fixed water depth (d) to the monopile radius (R) ratio. Apart from 4 wind farm sites with a large d/R ratio on the top left corner, the majority of the wind farms tend to have a similar d/R ratio and cluster towards the right bottom corner. This indicates there is a correlation between the monopile radius and relative water depths, which is expected as larger monopile foundations would be required for wind farms in deeper water.
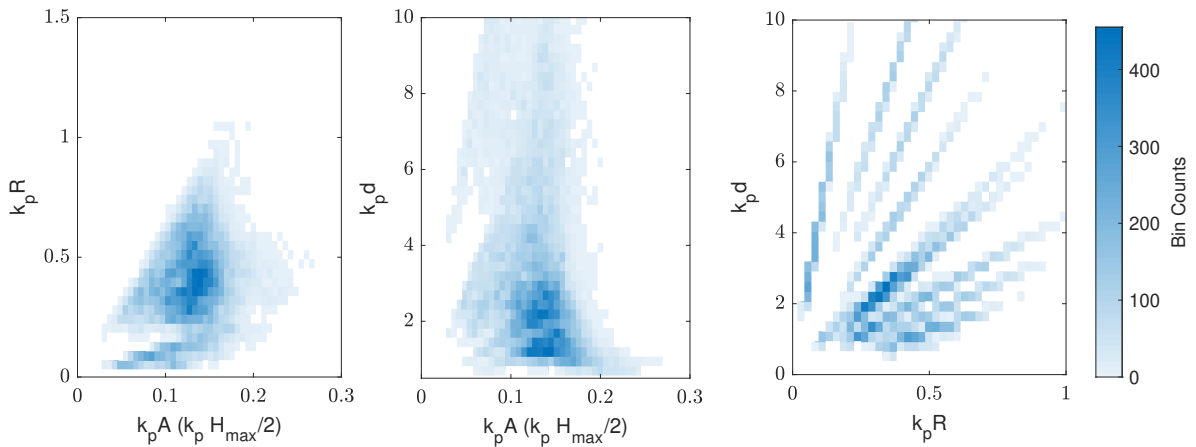

Figure 4: Bin scatter for sea-state parameters distributions between 2004 and 2024 for 36 locations of UK offshore wind farms.

7.2 Bayesian interference-based design

It is of interest to investigate how the GP model will design a new experiment based on previous experimental results. In this study, we assume that the peak wavenumber of these wave groups during experiments has a comparable wavenumber value to those extreme waves rising from the random sea-state with the same peak wavenumber. We have visualised the acquisition function for second order force coefficients for three water depths in Figure 5. As the acquisition function is assembled based on three parts: prediction residual, variance and conditional statistics from the metocean data (see details in section 6), a larger value in the acquisition function indicates a more important sampling region in the parameter space suggested by the GP model. This could be due to either less accurate predictions during cross-validation, uncertain predictions from the confidence interval or important sea-states that commonly occur in these wind farms (or maybe a combination).
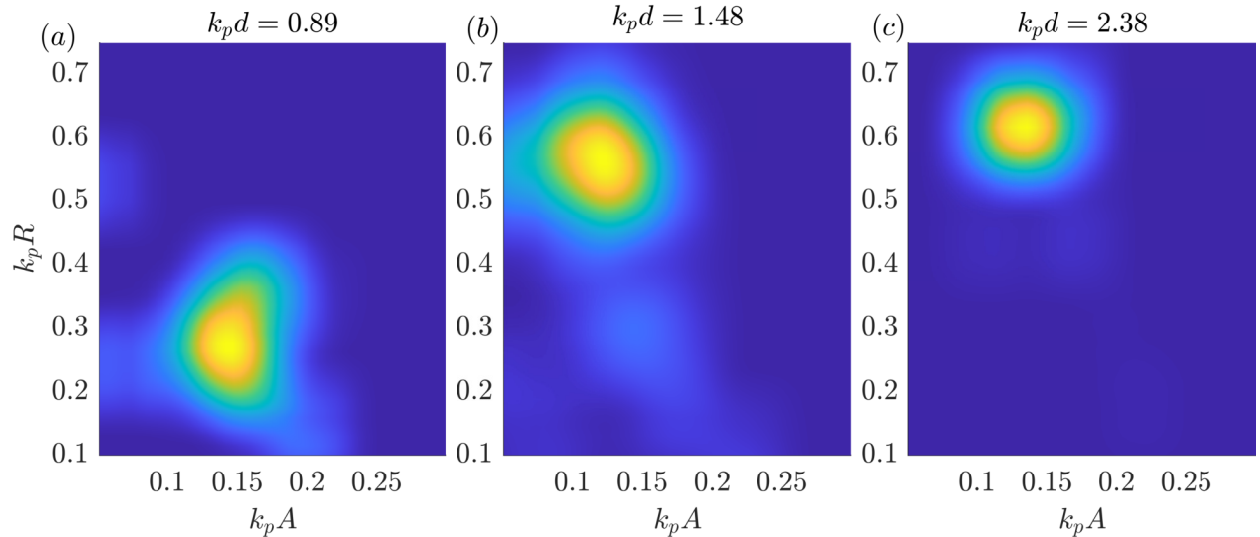

Figure 5: Visualisation of an example acquisition function for second order coefficients at different water depths. A moving average smooth function is applied herein with a smoothing window size of 4 data points.

The acquisition function from the GP model suggested low importance for the cases with k_pA values greater than 0.23 regardless of the value for k_pd and k_pR. This is simply because such very steep wave groups are unlikely to happen in the realistic water wave system, where wave breaking dissipates the energy and limits the maximum height. This constraint primarily comes from the conditional statistics of the sea-states input to the GP model. Additionally, the GP model also shows very limited importance for the cases with small k_pA values below 0.1 regardless of the value for k_pd and k_pR. This is expected as for these quasi-linear wave groups, the overall behaviour can be well captured very simply with small nonlinearity. It seems that the prior information provided from previous experiments is self-consistent based on cross-validation results and can provide sufficient data to make accurate predictions. GP model also shows increasing importance for the cases with larger k_pR values if the k_pd value increases. This could be because of the fact that for the wind farms in deeper waters, the radius of the monopile foundation is usually larger, and hence GP model weights the cases with a larger relative radius as more important to explore. It is also interesting to find out that the effect of k_pd on the nonlinear wave loading seems to have an asymptotic behaviour, where the importance (i.e. maximum of the acquisition function) shifts significantly from relatively shallow water to intermediate water depth from Figure 5 (a) to 5 (b) compared to the shift from intermediate water depth to relatively deep water ((b) to (c)).

Other physical constraints need to be considered in the design of such an experimental campaign. The first and foremost constraint comes from the fixed d/R ratio available for the test in the Strathclyde flume. This is similar to the fixed d/R ratio for the monopile foundations in UK-based wind farms. Varying the cylinder size simply requires replacing the cylinder and re-calibrate the load cells, which takes about an entire day to finish. Varying water depth is also difficult to achieve and further requires the re-calibration of wavemakers and wave probes. As such, instead of directly using the location in the parameter space, where the acquisition function reaches the maximum, finding the optimal d/R ratio is necessary. The final choice of cylinder radius is 0.2 meters as this is the maximum allowable size of the cylinder in the wave tank.
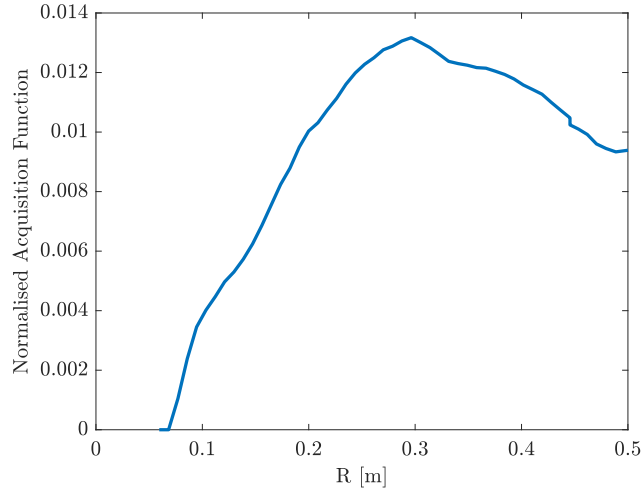
Figure 6: Integrated acquisition function for different values of cylinder radius based on the water depth of the flume $d = 1.8m$. Values of acquisition function are normalised by the triple integral along k_pA, k_pd and k_pR axis.

The final suggested Bayesian sampling points and the traditional grid search sampling points are shown in Figure 7. The sampling points based on the grid search method are determined based on intuition. Due to the fixed cylinder radius constraint, both experimental design approach results overlapped on the same d/R constant line in Figure 7 (c). We have also presented the test matrix of three previous experiments as the prior information. It seems that the current Bayesian sampling model focuses on a cluster region with less interest in exploring the short but steep wave region. This could be due to fewer short but steep sea states being observed in metocean data. It is interesting to find that during the experiments, some of the short but steep wave group designs shown in the top right corner of Figure 7 (a) suggested by the grid search method are not achievable as the wave breaks before reaching the cylinder, whereas the wave breaking causes less impact on the Bayesian sampled points.

7.3 Improvements in nonlinear load predictions

We now finally look at the sampling efficiency by comparing the novel metocean data integrated Bayesian sampling strategy against the traditional grid search method in this classic nonlinear wave loading prediction problem.

We first present the final prediction of the higher frequency components of nonlinear forces from the GP model trained from Bayesian sampling and from the traditional grid search design of the experiments in Figure 8. In general, both GP models perform well in capturing high-frequency nonlinear loads on a vertical cylinder. This could be attributed to the fact that the previous three experiments already provided a broad and sufficient sample. The GP model trained with Bayesian sampling outperforms slightly over the one trained with grid search design. The advantage of training with Bayesian sampling is more significant for the nonlinear force components with high frequencies as more noise is expected in these signals.

The results are also consistent for the k-fold cross-validated error (see details in Section 5) when predicting the second-order force amplitude coefficients shown in Figure 9. For both the Bayesian sampling method and the grid search method, the overall error is reduced when more experimental cases (i.e. new samples) are input into the training dataset. The Bayesian sampling strategy outperforms the traditional grid search sampling method based on purely physics intuition.

In this study, the primary objective of performing a new experiment is to better understand the variation of force amplitude coefficients in a given parameter space. A better understanding of force amplitude coefficient behaviours can directly improve the nonlinear force model prediction accuracy. The comparison results shown in Figure 8 clearly demonstrate the advantage of using a data-driven method to design a new experiment over the more classical ones, where the prediction model provides more accurate predictions on higher order harmonic forces. When the number of new experiments is fixed, following the wave group parameter suggested by the data-driven method can yield over 20% further improvement in the final force prediction accuracy as shown in Figure 9, which indicates that these experimental cases designed by the data-driven method provide better coverage of the parameter space with higher sampling efficiency.
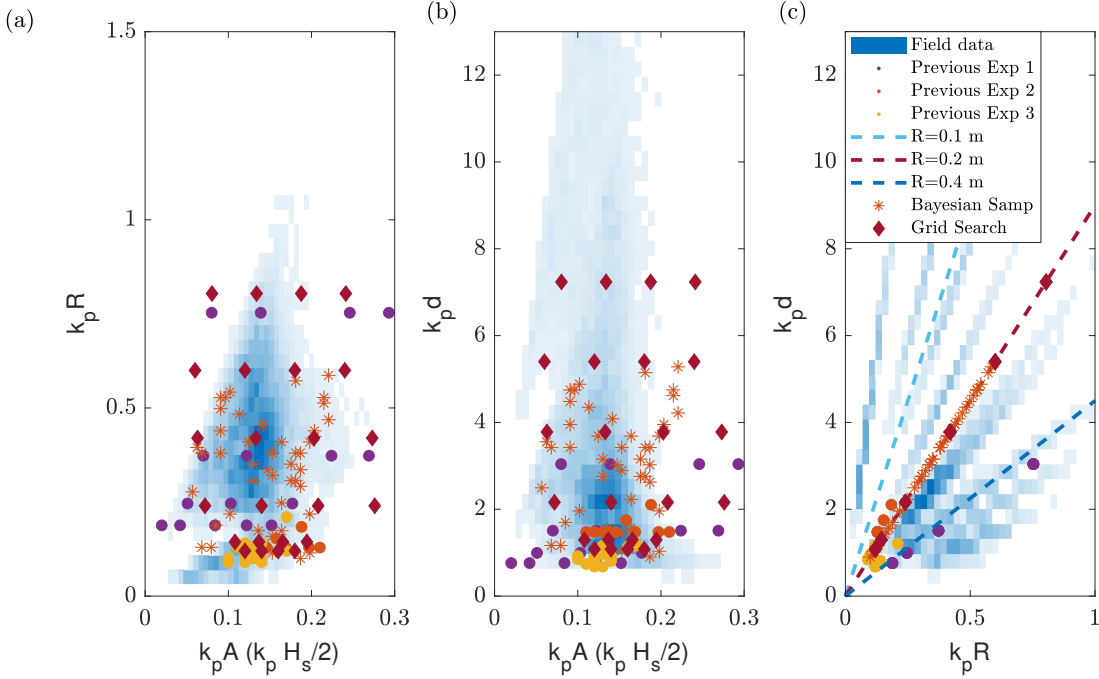
Figure 7: The design of bayesian sampling points for the new experiment at kelvin hydrodynamics laboratory, the University of Strathclyde. Three previous experimental data are obtained from (12; 13; 11) respectively. The constant radius-water depths lines are calculated based on the new experimental conditions (i.e. $d = 1.8m$).

8. Discussion and conclusions

In this paper, we present a Bayesian sampling-based experimental design strategy, which also incorporates metocean data as conditional statistics in a classic wave-structure interaction problem. Based on three previous experimental datasets as the prior information, a GP-based surrogate model is trained to predict the higher frequency force amplitude coefficients. An acquisition function is used to incorporate the metocean data into the experimental design. One of the critical experimental parameters – the size of the cylinder is optimised based on the proposed acquisition function with extra physical constrained imposed. New experiments are to be performed with wave group loads on a vertical cylinder at the University of Strathclyde. The GP model trained with Bayesian sampled experimental data shows a slight edge when compared to the traditional experimental design with grid search.

In this study, the modified acquisition function suggested by the machine learning model also helps us to rank the non-dimensional parameters in their space, each according to its importance. We found that the machine learning model can make interesting decisions which are compatible with physical intuition but in a more systematic way. For example, the machine learning model gives less importance to quasi-linear cases as these wave groups exhibit almost no nonlinear physics. The current machine learning model also gives less importance to strongly nonlinear cases, which avoid very short but steep wave group profiles. These wave groups are found later in the experiment to be impractical to investigate as the wave group will break before reaching the cylinder in the middle of the tank. It is worth mentioning that neither previous experiments nor metocean data are actually aimed at investigating wave breaking, but wave breaking occasionally affects both datasets.

Incorporating machine learning with metocean data is helpful in many aspects. Firstly, metocean data usually have a large amount of information with hidden underlying physics, data-driven methods could potentially better utilise this as an external source for experimental design (e.g. the current model avoids suggesting breaking cases). Secondly, metocean data also provides machine learning with real engineering conditions, which allows the decision to be made in a realistic way. The current model proposes increasing the monopile size in experiments when performed in deeper water, which superficially agrees with the current trend in the offshore wind industry. As such, we believe that the machine learning-assisted model could help to some extent with experimental design in a systemic manner.

In this study, we have also observed several challenges of implementing machine learning for a complete design of an experiment. This is primarily because the simplified acquisition function cannot take all the physical constraints into
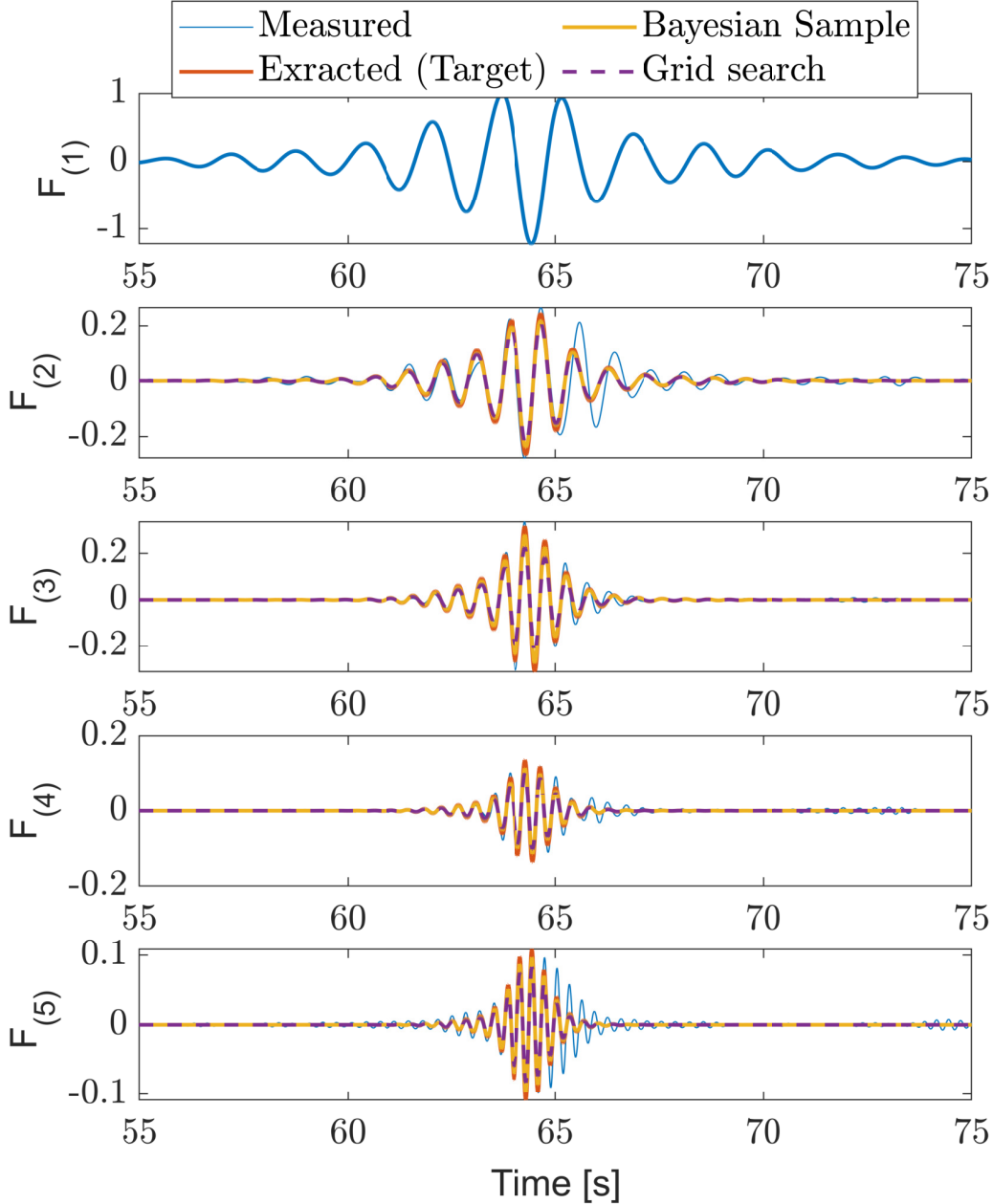
Figure 8: The final prediction of higher frequency components of nonlinear forces from the gp model trained from bayesian sampling suggested by surrogate model and grid search design of experiment.

consideration. For example, the GP model would suggest using 18 different sizes of cylinders for the optimal sampling strategy without considering the difficulties of varying the sizes and also the time taken to reinstall the cylinders. Manual modifications are still required for this study. However, it is possible to develop an improved acquisition function that provides a penalty when the size of the cylinder varies. This could minimise manual input and automate experimental design in the future. Additionally, the choice of experimental data is prior information and the metocean data could potentially introduce bias that leads to the designed experiment being suitable for a specific area but of less scientific interest (for example, less extreme conditions are considered for the GP model).

Finally, although these results need to be extrapolated with great care as limited data are available and from a single experimental campaign, the present paper serves as a case study for utilising machine learning tools to help design
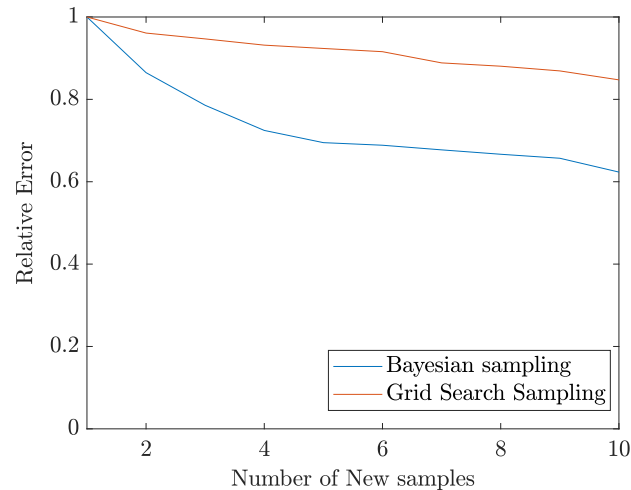
Figure 9: Relative prediction error evolution after new experimental data points are included in the training dataset.

model tests in ocean engineering. The challenge we have herein is common in ocean engineering–we have a large parameter space with various combinations of operating conditions to explore. However, the number of experimental or numerical runs is usually limited. To make full use of these tests, determining the representative cases becomes important for the design of model tests. Machine learning methods, as presented in this case study provide some useful insights into the experimental design as it allows the incorporation of field data. This also yields more accurate force predictions when compared to cases sampled using traditional approaches. The current data-informed model test design approach can be potentially extended to other ocean engineering practices.

Acknowledgements

References

[1] Kallehave, D., Byrne, B. W., LeBlanc Thilsted, C., and Mikkelsen, K. K., 2015, "Optimization of monopiles for offshore wind turbines," Philos. Trans. Royal Soc., **373**(2035), p. 20140100.

[2] Chaplin, J., Rainey, R., and Yemm, R., 1997, "Ringing of a vertical cylinder in waves," Journal of Fluid Mechanics, **350**, pp. 119–147.

[3] Grue, J. and Huseby, M., 2002, "Higher-harmonic wave forces and ringing of vertical cylinders," Applied ocean research, **24**(4), pp. 203–214.

[4] Riise, B. H., Grue, J., Jensen, A., and Johannessen, T. B., 2018, "A note on the secondary load cycle for a monopile in irregular deep water waves," J. Fluid Mech., **849**, p. R1.

[5] Kim, M.-H. and Yue, D. K., 1989, "The complete second-order diffraction solution for an axisymmetric body Part 1. Monochromatic incident waves," J. Fluid Mech., **200**, pp. 235–264.

[6] Huang, J. B. and Eatock Taylor, R., 1996, "Semi-analytical solution for second-order wave diffraction by a truncated circular cylinder in monochromatic waves," J. Fluid Mech., **319**, pp. 171–196.

[7] Faltinsen, O. M., Newman, J. N., and Vinje, T., 1995, "Nonlinear wave loads on a slender vertical cylinder," J. Fluid Mech., **289**, pp. 179–198.

[8] Molin, B. et al., 1995, "Third-harmonic wave diffraction by a vertical cylinder," J. Fluid Mech., **302**, pp. 203–229.

[9] Huseby, M. and Grue, J., 2000, "An experimental investigation of higher-harmonic wave forces on a vertical cylinder," J. Fluid Mech., **414**, pp. 75–103.

[10] Kristiansen, T. and Faltinsen, O. M., 2017, "Higher harmonic wave loads on a vertical cylinder in finite water depth," J. Fluid Mech., **833**, pp. 773–805.

[11] Mj, D., McAllister, M. L., Bredmose, H., Adcock, T. A. A., and Taylor, P. H., 2023, "Harmonic structure of wave loads on a surface piercing column in directionally spread and unidirectional random seas," J. Ocean Eng. Mar. Energy., pp. 1–19.

[12] Chen, L. F., Zang, J., Taylor, P. H., Sun, L., Morgan, G., Grice, J., Orszaghova, J., and Ruiz, M. T., 2018, "An experimental decomposition of nonlinear forces on a surface-piercing column: Stokes-type expansions of the force harmonics," J. Fluid Mech., **848**, pp. 42–77.

[13] Feng, X., Taylor, P. H., Dai, S., Day, A. H., Willden, R. H. J., and Adcock, T. A. A., 2020, "Experimental investigation of higher harmonic wave loads and moments on a vertical cylinder by a phase-manipulation method," Coast. Eng., **160**, p. 103747.

[14] Mockutė, A., Marino, E., Lugni, C., and Borri, C., 2019, "Comparison of nonlinear wave-loading models on rigid cylinders in regular waves," Energies, **12**(21), p. 4022.

[15] Stansberg, C. T., Huse, E., Krokstad, J. R., and Lehn, E., 1995, "Experimental study of non-linear loads on vertical cylinders in steep random waves," The Fifth International Offshore and Polar Engineering Conference, The Hague, The Netherlands, p. 824.

[16] Riise, B. H., Grue, J., Jensen, A., and Johannessen, T. B., 2018, "High frequency resonant response of a monopile in irregular deep water waves," Journal of Fluid Mechanics, **853**, pp. 564–586.

[17] Marino, E., Nguyen, H., Lugni, C., Manuel, L., and Borri, C., 2015, "Irregular nonlinear wave simulation and associated loads on offshore wind turbines," J. Offshore Mech. Arct., **137**(2), p. 021901.

[18] Schløer, S., Bredmose, H., and Bingham, H. B., 2016, "The influence of fully nonlinear wave forces on aero-hydro-elastic calculations of monopile wind turbines," Mar. Struct., **50**, pp. 162–188.

[19] Mohamad, M. A. and Sapsis, T. P., 2018, "Sequential sampling strategy for extreme event statistics in nonlinear dynamical systems," Proc. Natl. Acad. Sci. U. S. A., **115**(44), pp. 11138–11143.

[20] Sapsis, T. P., 2020, "Output-weighted optimal sampling for Bayesian regression and rare event statistics using few samples," Proc. R. Soc. A Math. Phys. Eng. Sci., **476**(2234), p. 20190834.

[21] Tang, T. and Adcock, T. A. A., 2022, "Estimating space–time wave statistics using a sequential sampling method and Gaussian process regression," Appl. Ocean Res., **122**, p. 103127.

[22] Gong, X. and Pan, Y., 2022, "Sequential Bayesian experimental design for estimation of extreme-event probability in stochastic input-to-response systems," Comput. Methods in Appl. Mech. Eng., **395**, p. 114979.

[23] Boccotti, P., 1983, "Some new results on statistical properties of wind waves," Appl. Ocean Res., **5**(3), pp. 134–140.

[24] Lindgren, G., 1970, "Some Properties of a Normal Process Near a Local Maximum," Ann. Math. Stat., **41**(6), pp. 1870–1883.

[25] Hasselmann, K., Barnett, T. P., Bouws, E., Carlson, H., Cartwright, D. E., Enke, K., Ewing, J., Gienapp, A., Hasselmann, D., Kruseman, P., et al., 1973, "Measurements of wind-wave growth and swell decay during the Joint North Sea Wave Project (JONSWAP)." Ergaenzungsheft zur Deutschen Hydrographischen Zeitschrift, Reihe A.

[26] Lo, E. and Mei, C. C., 1985, "A numerical study of water-wave modulation based on a higher-order nonlinear Schrödinger equation," J. Fluid Mech., **150**, pp. 395–416.

[27] Baldock, T. E., Swan, C., and Taylor, P. H., 1996, "A laboratory study of nonlinear surface waves on water," Philos. Trans. Royal Soc. A Math. Phys. Eng. Sci., **354**(1707), pp. 649–676.

[28] Adcock, T. A. A. and Taylor, P. H., 2009, "Focusing of unidirectional wave groups on deep water: an approximate nonlinear Schrödinger equation-based model," Proc. R. Soc. A Math. Phys. Eng. Sci., **465**(2110), pp. 3083 LP – 3102.

[29] Janssen, T. T. and Herbers, T. H. C., 2009, "Nonlinear Wave Statistics in a Focal Zone," J. Phys. Oceanogr., **39**(8), pp. 1948–1964.

[30] Hersbach, H., Bell, B., Berrisford, P., Hirahara, S., Horányi, A., Muñoz-Sabater, J., Nicolas, J., Peubey, C., Radu, R., Schepers, D., et al., 2020, "The ERA5 global reanalysis," Q. J. R. Meteorol. Soc., **146**(730), pp. 1999–2049.

[31] Wang, S., Larsen, T. J., and Bredmose, H., 2021, "Ultimate load analysis of a 10 MW offshore monopile wind turbine incorporating fully nonlinear irregular wave kinematics," Mar. Struct., **76**, p. 102922.

[32] Fitzgerald, C. J., Taylor, P. H., Eatock Taylor, R., Grice, J., and Zang, J., 2014, "Phase manipulation and the harmonic components of ringing forces on a surface-piercing column," Proc. R. Soc. A, **470**(2168), p. 20130847.

[33] Durbin, J. and Koopman, S. J., 2012, *Time series analysis by state space methods*, Vol. 38, OUP Oxford.

[34] Kocijan, J., Murray-Smith, R., Rasmussen, C. E., and Girard, A., 2004, "Gaussian process model based predictive control," *Proceedings of the 2004 American control conference*, Vol. 3, IEEE, pp. 2214–2219.

[35] Hewing, L., Kabzan, J., and Zeilinger, M. N., 2019, "Cautious model predictive control using gaussian process regression," IEEE Transactions on Control Systems Technology, **28**(6), pp. 2736–2743.

[36] Gramstad, O., Agrell, C., Bitner-Gregersen, E., Guo, B., Ruth, E., and Vanem, E., 2020, "Sequential sampling method using Gaussian process regression for estimating extreme structural response," Mar. Struct., **72**, p. 102780.

[37] Rasmussen, C. E. and Williams, C., 2006, "Gaussian processes for machine learning, ser. Adaptive computation and machine learning," Cambridge, MA, USA: MIT Press, **38**, pp. 715–719.

[38] Rodriguez, J. D., Perez, A., and Lozano, J. A., 2009, "Sensitivity analysis of k-fold cross validation in prediction error estimation," IEEE Trans. Pattern Anal. Mach. Intell., **32**(3), pp. 569–575.

[39] Blanchard, A. and Sapsis, T., 2021, "Bayesian optimization with output-weighted optimal sampling," J. Comput. Phys., **425**, p. 109901.

[40] Pickering, E., Guth, S., Karniadakis, G. E., and Sapsis, T. P., 2022, "Discovering and forecasting extreme events via active learning in neural operators," Nat. Comput. Sci, **2**(12), pp. 823–833.

[41] Onorato, M., Waseda, T., Toffoli, A., Cavaleri, L., Gramstad, O., Janssen, P. A. E. M., Kinoshita, T., Monbaliu, J., Mori, N., Osborne, A. R., et al., 2009, "Statistical properties of directional ocean waves: the role of the modulational instability in the formation of extreme events," Phys. Rev. Lett,, **102**(11), p. 114502.